Comput Mech (2009) 43:715–730
DOI 10.1007/s00466-008-0340-9

ORIGINAL PAPER

Mixed finite element formulation for the general anti-plane shear problem, including mode III crack computations, in the framework of dipolar linear gradient elasticity

S. I. Markolefas · D. A. Tsouvalas · G. I. Tsamasphyros

Received: 28 February 2008 / Accepted: 11 September 2008 / Published online: 21 October 2008

Abstract A mixed formulation is developed and numerically validated for the general 2D anti-plane shear problem in micro-structured solids governed by *dipolar strain gradient elasticity*. The current mixed formulation employs the form II statement of the gradient elasticity theory and uses the double stress components and the displacement field as main variables. High order, C^0-continuous, conforming basis functions are employed in the finite element approximations (p-version). The results for the mode III crack problem reveal that, with proper mesh refinement at the areas of high solution gradients, the current approximation method captures the exact solution behaviour at different length scales, which depend on the size of material micro-structure. The latter is of vital importance because, near the crack tip, the nature of the exact solution, changes radically as we proceed from the *macro*- to *micro*-scale.

Keywords Dipolar strain gradient elasticity · Mixed formulations · Mixed finite elements · p-Version

1 Introduction

The goal of the present work is the development and numerical verification of a *mixed formulation* for the general 2D *anti-plane shear* problem in micro-structured solids governed by *dipolar strain gradient elasticity* (strain gradient theory of grade-two [4,15]). The proposed mixed formulation employs the form II statement of the gradient elasticity theory. The main variables are the *double stress tensor* and the *displacement* field. The current formulation falls in the general category of mixed methods developed in [13], see also [3,12,18]. The solution function spaces are appropriately defined and the final weak forms have the standard (symmetric) mixed structure. High order, C^0-continuous, conforming basis functions are employed in the finite element approximations (p-version or p-extension), see Sect. 4 for details.

Mixed finite element methods for strain gradient elasticity and couple stress problems, employing different sets of main variables from those used herein, are also developed in [1]. Boundary element techniques may be found in [10,16]. Analytical methods for the mode III crack problem, in the framework of Form II strain gradient elasticity, are given in [7]. Closed form solutions for the same problem, in the framework of couple stress theory are contained in [9,19].

The practical necessity of strain gradient theories is justified by experimental studies, which reveal that the material behaviour at micro-scale is significantly different from that of the bulk material. More precisely, when the characteristic length scale of the experiment is comparable to the intrinsic length of the microstructure, strong size effects are present (e.g., bending of ultra-thin beams [8,11]). Even for large scale structures, the gradient effects become important near areas with steep gradients of the strain (like corners, cracks, etc.).

The results for the mode III crack problem (Sect. 4) show that, with proper mesh refinement at the areas of high solution gradients, the current approximation method captures the exact solution behaviour at both micro- and macro-scales. The latter is very important because, near the crack tip, the nature of the exact solution (for both *true* stress and displacement fields), changes radically as we proceed from the *macro*- to *micro*-scale, where the strain gradient effects dominate the phenomena [7,9,11,19].

S. I. Markolefas (✉) · D. A. Tsouvalas · G. I. Tsamasphyros
Department of Applied Mechanics, Faculty of Applied Mathematics and Physics, National Technical University of Athens, 9 Iroon Polytechniou, Zografou, 157 73 Athens, Greece
e-mail: markos34@gmail.com

The basic characteristic of the *gradient elasticity* theory (as well as, the main departure from *classical elasticity*) is that the *strain energy density* is a *positive-definite* functional of the standard strain (as in the classical elasticity), as well as, of the second gradient of the displacement field (*Form I*) or the first gradient of strain (*Form II*). The new material constants introduced contain certain *characteristic lengths*, related to the size and topology of the micro-structure. In this way, size effects are incorporated in the stress analysis. Typical real materials that can be modeled are materials with periodic microstructure like *crystals* (crystal lattices), *polycrystal materials* (crystallites), *polymers* (molecules) and *granular material* (grains); the respective micro-media are given in the parentheses [14].

Summarizing, the paper is organized into the following parts: Sect. 2 introduces the governing equations and boundary conditions of the anti-plane shear problem in the framework of strain (dipolar) gradient elasticity. The proposed mixed formulation is developed in Sect. 3. Section 4 contains the results from the numerical experimentations. Finally, concluding remarks are given in Sect. 5.

2 Governing equations and boundary conditions

The detailed description of the assumptions leading to the governing equations of 2D anti-plane shear problem, based on the general 3D dipolar gradient elasticity theory, may be found in [7]. In the following we outline the results that will be used in Sect. 3, in order to develop the mixed formulation of the present work.

A pure anti-plane shear state is reached if the body has the form of a thick slab in the z-direction (Fig. 1). Moreover, the external tractions act along the z-direction. Considering unit width along the z-direction, the following two-dimensional displacement field is generated,

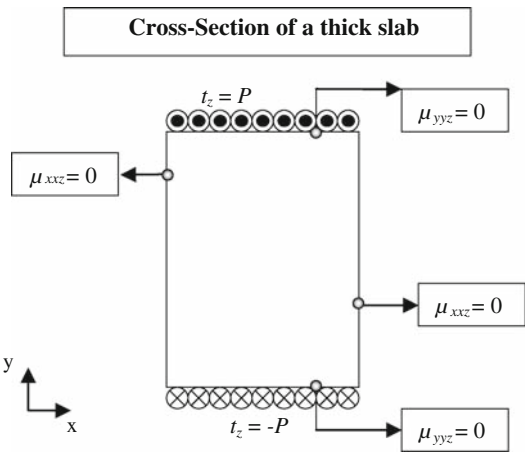

Fig. 1 Anti-plane shear boundary value problem description

$$u_x = u_y = 0 \tag{2.1a}$$

$$u_z = w(x, y) \tag{2.1b}$$

where $w(x, y)$ is a scalar valued function of two independent variables, $(x, y) \in \Omega$ (Ω denotes the problem domain); representing the out-of-plane displacement field.

Assuming isotropic constitutive relations (hence, there are no coupling terms between standard and double stresses [13,14]), the following stress-strain relations may be stated for the non-vanishing stress components in a given Cartesian coordinate system x, y, z,

Standard (monopolar) Cauchy stresses:

$$\tau_{xz} = \mu \frac{\partial w}{\partial x} = \tau_{13} \tag{2.2a}$$

$$\tau_{yz} = \mu \frac{\partial w}{\partial y} = \tau_{23} \tag{2.2b}$$

Double (dipolar) stresses:

$$\mu_{xxz} = \mu c \frac{\partial^2 w}{\partial x^2} = \mu_{113} \tag{2.3a}$$

$$\mu_{xyz} = \mu c \frac{\partial^2 w}{\partial x \partial y} = \mu_{123} \tag{2.3b}$$

$$\mu_{yxz} = \mu c \frac{\partial^2 w}{\partial y \partial x} = \mu_{213} \tag{2.3c}$$

$$\mu_{yyz} = \mu c \frac{\partial^2 w}{\partial y^2} = \mu_{223} \tag{2.3d}$$

where $\mu > 0$ is the standard shear modulus [Force/Length^2] and $c > 0$ is a (small) constant (the so-called, gradient coefficient [Length^2]), related to the nature of the material microstructure. The definition, as well as the physical meaning of the double stress components may be found in [14].

According to [7], $c = O(0.1h^2)$, where h is an intrinsic material length, while according to [19], $c \approx 0.50l^2$, where l is a characteristic material length. Both h and l are directly associated with the size of the material microstructure.

The so-called Form II formulation has been employed in the development of the above equations [7,15]. The symmetries $\mu_{ijk} = \mu_{ikj}$, encountered in the Form II statement of the gradient elasticity theory, have already been taken into account. On the other hand, it is well known that $\frac{\partial^2 w}{\partial x \partial y} = \frac{\partial^2 w}{\partial y \partial x}$ in the *sense of distributions*, hence $\mu_{xyz} = \mu_{yxz}$, as well. However, in a general Form II formulation it holds that $\mu_{xyz} \neq \mu_{yxz}$. Therefore, for the purpose of generality, we currently consider them as independent variables.

Using (2.2), (2.3) and the equilibrium equations of the dipolar gradient elasticity theory [4,13,15], the following

fourth order governing differential equation is derived, see [7] for details,

$$c\nabla^4 w - \nabla^2 w = 0 \tag{2.4}$$

where $\nabla^2 := (\frac{\partial^2}{\partial x^2}) + (\frac{\partial^2}{\partial y^2})$ and $\nabla^4 := \nabla^2 \cdot \nabla^2$.

The above partial differential equation is accompanied by suitable boundary conditions. The structure of the boundary conditions, which depend on the particular application, may be deduced by proper reduction from the general gradient elasticity boundary conditions [4,13,15]. Assuming that the surface double traction, as well as, the body double force are absent, the proper boundary conditions are as follows [13]:

Traction boundary conditions:

$$n_j(\tau_{jk} - \partial_i \mu_{ijk}) - D_j(n_i \mu_{ijk}) + (D_l n_l) n_j n_i \mu_{ijk} = t_k \quad \text{on } S^k_{N,t} \tag{2.5a}$$

Moment boundary conditions:

$$n_i n_j \mu_{ijk} = 0 \quad \text{on } S^k_{N,m} \tag{2.5b}$$

Jump conditions:

$$[m_j n_i \mu_{ijk}] = 0 \quad \text{on } C \tag{2.5c}$$

where

n_j: components of the outer unit vector normal to the surface.

τ_{ij}: components of the (symmetric) *Cauchy* stress tensor.

μ_{ijk}: components of the double stress tensor (moment per unit area).

t_k: components of surface (true) traction (force per unit area).

$D_j(*) := (\delta_{jl} - n_j n_l)\partial_l(*)$: surface gradient operator.

δ_{jl} : Components of K*ronecker* delta operator.

C: collectively denotes the curve(s) on the boundary where the normal unit vectors exhibit jumps (i.e., corners, edges, etc.).

$[y]$: the difference of the values of quantity y between both sides of curve C.

$m_j := e_{lkj} s_l n_k$: where s_l denotes the components of the tangential vector of curve C and e_{lkj} is the well known *alternating tensor*.

$S^k_{N,t}$: part of the boundary where the k component of the right hand side of the traction condition (2.5a) is specified (a given point of the boundary either belongs to $S^k_{N,t}$ or the displacement field u_k must be specified on this point).

$S^k_{N,m}$: part of the boundary where the k component of the right hand side of the moment condition (2.5b) is specified (a given point of the boundary either belongs to $S^k_{N,m}$ or the normal derivative $Du_k := n_l \partial_l u_k$ must be specified on this point).

Denoting by $S^k_{E,t}$ the boundary part where u_k is prescribed and $S^k_{E,m}$ the part where Du_k is specified, it holds that $S^k_{N,t} \cup S^k_{E,t} = S$, $S^k_{N,t} \cap S^k_{E,t} = \emptyset$ and $S^k_{N,m} \cup S^k_{E,m} = S$, $S^k_{N,m} \cap S^k_{E,m} = \emptyset$. Only zero (homogeneous) essential conditions are considered herein. Moreover, in the following we use the symbols x, y, z instead of 1, 2, 3 of the indicial notation.

Assuming for simplicity that the boundary curves are straight lines parallel to x or y axis, see Fig. 1 and using (2.5), the following boundary condition cases can be formulated for the general anti-plane shear problem. We omit the intermediate algebra.

(1) Boundary curve which is part of $S^3_{N,t}$ and parallel to the y axis, with applied true traction $t_3 \equiv t_z$, along z axis

$$t_z = \left(\tau_{xz} - \frac{\partial \mu_{xxz}}{\partial x} - \frac{\partial \mu_{yxz}}{\partial y} - \frac{\partial \mu_{xyz}}{\partial y}\right) n_x \tag{2.6}$$

(2) Boundary curve which is part of $S^3_{N,t}$ and parallel to the x axis, with applied true traction $t_3 \equiv t_z$, along z axis

$$t_z = \left(\tau_{yz} - \frac{\partial \mu_{xyz}}{\partial x} - \frac{\partial \mu_{yyz}}{\partial y} - \frac{\partial \mu_{yxz}}{\partial x}\right) n_y \tag{2.7}$$

(3) Boundary curve which is part of $S^3_{N,m}$ and parallel to the y axis

$$\mu_{xxz} = 0 \tag{2.8}$$

(4) Boundary curve which is part of $S^3_{N,m}$ and parallel to the x axis

$$\mu_{yyz} = 0 \tag{2.9}$$

(5) Boundary curve which is part of $S^3_{E,t}$ and parallel to the x or y axis

$$u_z = 0 \tag{2.10}$$

(6) Boundary curve which is part of $S^3_{E,m}$ and parallel to the y axis

$$\frac{\partial u_z}{\partial x} = 0 \tag{2.11}$$

(7) Boundary curve which is part of $S^3_{E,m}$ and parallel to the x axis

$$\frac{\partial u_z}{\partial y} = 0 \tag{2.12}$$

(8) Jump conditions at the (right angle) corners, see (2.5c) and Appendix I

$$\mu_{xyz} + \mu_{yxz} = 0 \Rightarrow \mu_{xyz} = \mu_{yxz} = 0 \tag{2.13}$$

(9) *Anti-symmetry conditions*:
If a parallel to x axis boundary line is an axis of anti-symmetry, then

$$\mu_{yyz} = 0 \tag{2.14}$$

If a parallel to y axis boundary line is an axis of anti-symmetry, then

$$\mu_{xxz} = 0 \tag{2.15}$$

(10) *Symmetry conditions:*
If a parallel to x axis boundary line is an axis of symmetry, then

$$\mu_{yxz} = 0 \tag{2.16}$$

If a parallel to y axis boundary line is an axis of symmetry, then

$$\mu_{xyz} = 0 \tag{2.17}$$

3 Formulation of the mixed method

Let $r_{xxz}, r_{xyz}, r_{yxz}, r_{yyz}$ be proper *weighting functions* associated with the double stresses given by (2.3). The following integral equations may be formed:

$$\int_\Omega \frac{r_{xxz}\mu_{xxz}}{\mu c}\mathrm{d}\Omega = \int_\Omega r_{xxz}\frac{\partial^2 w}{\partial x^2}\mathrm{d}\Omega \tag{3.1a}$$

$$\int_\Omega \frac{r_{xyz}\mu_{xyz}}{\mu c}\mathrm{d}\Omega = \int_\Omega r_{xyz}\frac{\partial^2 w}{\partial x \partial y}\mathrm{d}\Omega \tag{3.1b}$$

$$\int_\Omega \frac{r_{yxz}\mu_{yxz}}{\mu c}\mathrm{d}\Omega = \int_\Omega r_{yxz}\frac{\partial^2 w}{\partial y \partial x}\mathrm{d}\Omega \tag{3.1c}$$

$$\int_\Omega \frac{r_{yyz}\mu_{yyz}}{\mu c}\mathrm{d}\Omega = \int_\Omega r_{yyz}\frac{\partial^2 w}{\partial y^2}\mathrm{d}\Omega \tag{3.1d}$$

Employing the standard Gauss theorem in (3.1) there follows,

$$\int_\Omega \frac{r_{xxz}\mu_{xxz}}{\mu c}\mathrm{d}\Omega = \int_S r_{xxz}\frac{\partial w}{\partial x}n_x \mathrm{d}S - \int_\Omega \frac{\partial r_{xxz}}{\partial x}\frac{\partial w}{\partial x}\mathrm{d}\Omega \tag{3.2a}$$

$$\int_\Omega \frac{r_{xyz}\mu_{xyz}}{\mu c}\mathrm{d}\Omega = \int_S r_{xyz}\frac{\partial w}{\partial y}n_x \mathrm{d}S - \int_\Omega \frac{\partial r_{xyz}}{\partial x}\frac{\partial w}{\partial y}\mathrm{d}\Omega \tag{3.2b}$$

$$\int_\Omega \frac{r_{yxz}\mu_{yxz}}{\mu c}\mathrm{d}\Omega = \int_S r_{yxz}\frac{\partial w}{\partial x}n_y \mathrm{d}S - \int_\Omega \frac{\partial r_{yxz}}{\partial y}\frac{\partial w}{\partial x}\mathrm{d}\Omega \tag{3.2c}$$

$$\int_\Omega \frac{r_{yyz}\mu_{yyz}}{\mu c}\mathrm{d}\Omega = \int_S r_{yyz}\frac{\partial w}{\partial y}n_y \mathrm{d}S - \int_\Omega \frac{\partial r_{yyz}}{\partial y}\frac{\partial w}{\partial y}\mathrm{d}\Omega \tag{3.2d}$$

Adding (3.2a–d), the following weak equation is formed,

$$\begin{aligned}\int_\Omega \frac{(r_{xxz}\mu_{xxz} + r_{xyz}\mu_{xyz} + r_{yxz}\mu_{yxz} + r_{yyz}\mu_{yyz})}{\mu c}\mathrm{d}\Omega \\ + \int_\Omega \left(\frac{\partial r_{xxz}}{\partial x}\frac{\partial w}{\partial x} + \frac{\partial r_{xyz}}{\partial x}\frac{\partial w}{\partial y} + \frac{\partial r_{yxz}}{\partial y}\frac{\partial w}{\partial x}\right. \\ \left. + \frac{\partial r_{yyz}}{\partial y}\frac{\partial w}{\partial y}\right)\mathrm{d}\Omega \\ = \int_S \left(r_{xxz}\frac{\partial w}{\partial x}n_x + r_{xyz}\frac{\partial w}{\partial y}n_x\right. \\ \left. + r_{yxz}\frac{\partial w}{\partial x}n_y + r_{yyz}\frac{\partial w}{\partial y}n_y\right)\mathrm{d}S\end{aligned} \tag{3.3}$$

Depending on the direction of the unit, outward, normal vector, some of the boundary terms in (3.3) are known a priori (thus, they remain in the forcing functional), while other boundary terms contribute to the bilinear functional. For example, if part of the boundary is parallel to the y axis, i.e., $n_x = +1$ or $n_x = -1$, the respective contribution of the term $\int_S \left(r_{xxz}\frac{\partial w}{\partial x}n_x\right) dS$ is known a priori; since, from the *double traction (moment) condition* (2.5b), either $Dw = \frac{\partial w}{\partial x}$ or μ_{xxz} is known (in the latter case $r_{xxz} = 0$, as usually considered in the weighted residual methods). Moreover, the term $\int_S \left(r_{xyz}\frac{\partial w}{\partial y}n_x\right) dS$ is not known a priori and must be transferred to the left hand side of the weak equation (it contributes to the stiffness matrix of the respective finite element approximation, see Sect. 4).

Note that for boundary curves which are not aligned with x or y axis, one has to write each partial derivative as the sum of normal and tangential derivatives, see [13] and Sect. 2. Next we consider the equilibrium equation, which leads to (2.4), see [7], for details.

$$\frac{\partial}{\partial x}\left(\tau_{xz}-\frac{\partial \mu_{xxz}}{\partial x}-\frac{\partial \mu_{yxz}}{\partial y}\right)+\frac{\partial}{\partial y}\left(\tau_{yz}-\frac{\partial \mu_{xyz}}{\partial x}-\frac{\partial \mu_{yyz}}{\partial y}\right)=0 \tag{3.4}$$

Let s be a proper *weighting function* for the displacement field w. Then, multiplying (3.4) by s, integrating over the problem domain and using the Gauss' theorem, it follows,

$$\begin{aligned}\int_\Omega\left(\frac{\partial s}{\partial x}\frac{\partial \mu_{xxz}}{\partial x}+\frac{\partial s}{\partial x}\frac{\partial \mu_{yxz}}{\partial y}+\frac{\partial s}{\partial y}\frac{\partial \mu_{xyz}}{\partial x}+\frac{\partial s}{\partial y}\frac{\partial \mu_{yyz}}{\partial y}\right)\mathrm{d}\Omega\\ -\int_\Omega\left(\frac{\partial s}{\partial x}\mu\frac{\partial w}{\partial x}+\frac{\partial s}{\partial y}\mu\frac{\partial w}{\partial y}\right)\mathrm{d}\Omega\\ =-\int_S s\left(\tau_{xz}-\frac{\partial \mu_{xxz}}{\partial x}-\frac{\partial \mu_{yxz}}{\partial y}\right)n_x\mathrm{d}S\\ -\int_S s\left(\tau_{yz}-\frac{\partial \mu_{xyz}}{\partial x}-\frac{\partial \mu_{yyz}}{\partial y}\right)n_y\mathrm{d}S\end{aligned} \tag{3.5}$$

The (*true*) *traction condition*, for straight boundary lines aligned with x or y axis (which are parts of $S^3_{N,t}$), is written as follows:

$$\begin{aligned}t_z=&\left(\tau_{xz}-\frac{\partial \mu_{xxz}}{\partial x}-\frac{\partial \mu_{yxz}}{\partial y}-\frac{\partial \mu_{xyz}}{\partial y}\right)n_x\\ &+\left(\tau_{yz}-\frac{\partial \mu_{xyz}}{\partial x}-\frac{\partial \mu_{yyz}}{\partial y}-\frac{\partial \mu_{yxz}}{\partial x}\right)n_y\end{aligned} \tag{3.6}$$

where t_z is the externally applied (*true*) *traction* along the z axis, see Fig. 1.

Using (3.6), the right-hand side of the weak equation (3.5) takes a more familiar form,

$$G(s)=-\int_S st_z\mathrm{d}S-\int_S s\frac{\partial \mu_{xyz}}{\partial y}n_x\mathrm{d}S-\int_S s\frac{\partial \mu_{yxz}}{\partial x}n_y\mathrm{d}S \tag{3.7}$$

The boundary terms appearing in (3.7) depend on tangential derivatives of the double stresses μ_{xyz} and μ_{yxz}. Applying the surface divergence theorem [4,14], one may show that,

$$\begin{aligned}-\int_S s\frac{\partial \mu_{xyz}}{\partial y}n_x\mathrm{d}S-\int_S s\frac{\partial \mu_{yxz}}{\partial x}n_y\mathrm{d}S\\ =\int_S\frac{\partial s}{\partial y}\mu_{xyz}n_x\mathrm{d}S+\int_S\frac{\partial s}{\partial x}\mu_{yxz}n_y\mathrm{d}S\end{aligned} \tag{3.8}$$

hence,

$$G(s)=-\int_S st_z\mathrm{d}S+\int_S\frac{\partial s}{\partial y}\mu_{xyz}n_x\mathrm{d}S+\int_S\frac{\partial s}{\partial x}\mu_{yxz}n_y\mathrm{d}S \tag{3.9}$$

The jump condition (2.5c) has been employed in (3.8), see also (2.13) and Appendix I. It is not difficult to see that the boundary terms on the right-hand side of (3.8) are conjugate to the boundary terms of (3.3), which are not known a priori. Now we are in the position to demonstrate the final structure of the current mixed formulation.

Mixed formulation 3.1. Find $(\mu_{xxz},\mu_{xyz},\mu_{yxz},\mu_{yyz})$ belonging to $Z\subset H^1(\Omega)^4$ and $w\in X\subset H^1(\Omega)$ such that

$$\begin{aligned}\int_\Omega\frac{(r_{xxz}\mu_{xxz}+r_{xyz}\mu_{xyz}+r_{yxz}\mu_{yxz}+r_{yyz}\mu_{yyz})}{\mu c}\mathrm{d}\Omega\\ +\int_\Omega\left(\frac{\partial r_{xxz}}{\partial x}\frac{\partial w}{\partial x}+\frac{\partial r_{xyz}}{\partial x}\frac{\partial w}{\partial y}+\frac{\partial r_{yxz}}{\partial y}\frac{\partial w}{\partial x}\right.\\ \left.+\frac{\partial r_{yyz}}{\partial y}\frac{\partial w}{\partial y}\right)\mathrm{d}\Omega-\int_S\left(r_{xyz}\frac{\partial w}{\partial y}n_x+r_{yxz}\frac{\partial w}{\partial x}n_y\right)\mathrm{d}S\\ =\int_S\left(r_{xxz}\frac{\partial w}{\partial x}n_x+r_{yyz}\frac{\partial w}{\partial y}n_y\right)\mathrm{d}S\end{aligned} \tag{3.10}$$

for every $(r_{xxz},r_{xyz},r_{yxz},r_{yyz})$ belonging to $U\subset H^1(\Omega)^4$ and

$$\begin{aligned}\int_\Omega\left(\frac{\partial s}{\partial x}\frac{\partial \mu_{xxz}}{\partial x}+\frac{\partial s}{\partial x}\frac{\partial \mu_{yxz}}{\partial y}+\frac{\partial s}{\partial y}\frac{\partial \mu_{xyz}}{\partial x}+\frac{\partial s}{\partial y}\frac{\partial \mu_{yyz}}{\partial y}\right)\mathrm{d}\Omega\\ -\int_S\frac{\partial s}{\partial y}\mu_{xyz}n_x\mathrm{d}S-\int_S\frac{\partial s}{\partial x}\mu_{yxz}n_y\mathrm{d}S\\ -\int_\Omega\left(\frac{\partial s}{\partial x}\mu\frac{\partial w}{\partial x}+\frac{\partial s}{\partial y}\mu\frac{\partial w}{\partial y}\right)\mathrm{d}\Omega=-\int_S st_z\mathrm{d}S\end{aligned} \tag{3.11}$$

for every $s\in Q\subset H^1(\Omega)$.

Assuming that $(\mu_{xxz},\mu_{xyz},\mu_{yxz},\mu_{yyz})$ and w vanish at the respective essential boundaries (i.e., $Z=U$ and $X=Q$) the above mixed formulation has the following standard structure of the general theory of mixed methods [2,5,6]

Find $\mu:=(\mu_{xxz},\mu_{xyz},\mu_{yxz},\mu_{yyz})\in U$ and $w\in Q$ such that

$$A(\mu,r)+B(r,w)=F(r),\quad \forall r\in U \tag{3.12a}$$

$$B(\mu,s)-C(w,s)=G(s),\quad \forall s\in Q \tag{3.12b}$$

where $r:=(r_{xxz},r_{xyz},r_{yxz},r_{yyz})\in U$

Note that the bilinear form $A(\mu,r)$ is coercive (hence positive definite) on the space $L^2(\Omega)^4$ and the bilinear form $C(w,s)$ is coercive on Q (assuming non-zero essential conditions for the displacement field, i.e., no rigid body motions). Mathematical analysis regarding solution existence, uniqueness and stability of the above mixed formulation can be found in [3,13].

Table 1 The stiffness matrix of the mixed finite element formulation

	$\mu_{xxz}\,(N_{1j})$	$\mu_{xyz}\,(N_{2j})$	$\mu_{yxz}\,(N_{3j})$	$\mu_{yyz}\,(N_{4j})$	$w\,(N_{5j})$
$r_{xxz}\,(N_{1i})$	$\int_\Omega \frac{N_{1i}N_{1j}}{\mu c}\mathrm{d}\Omega$	0	0	0	$\int_\Omega N_{1i,x}N_{5j,x}\mathrm{d}\Omega$
$r_{xyz}\,(N_{2i})$	0	$\int_\Omega \frac{N_{2i}N_{2j}}{\mu c}\mathrm{d}\Omega$	0	0	$\int_\Omega N_{2i,x}N_{5j,y}\mathrm{d}\Omega - \int_S N_{2i}N_{5j,y}n_x\mathrm{d}S$
$r_{yxz}\,(N_{3i})$	0	0	$\int_\Omega \frac{N_{3i}N_{3j}}{\mu c}\mathrm{d}\Omega$	0	$\int_\Omega N_{3i,y}N_{5j,x}\mathrm{d}\Omega - \int_S N_{3i}N_{5j,x}n_y\mathrm{d}S$
$r_{yyz}\,(N_{4i})$	0	0	0	$\int_\Omega \frac{N_{4i}N_{4j}}{\mu c}\mathrm{d}\Omega$	$\int_\Omega N_{4i,y}N_{5j,y}\mathrm{d}\Omega$
$s(N_{5i})$	$\int_\Omega N_{5i,x}N_{1j,x}\mathrm{d}\Omega$	$\int_\Omega N_{5i,y}N_{2j,x}\mathrm{d}\Omega$ $-\int_S N_{5i,y}N_{2j}n_x\mathrm{d}S$	$\int_\Omega N_{5i,x}N_{3j,y}\mathrm{d}\Omega$ $-\int_S N_{5i,x}N_{3j}n_y\mathrm{d}S$	$\int_\Omega N_{5i,y}N_{4j,y}\mathrm{d}\Omega$	$-\int_\Omega N_{5i,x}\mu N_{5j,x}\mathrm{d}\Omega$ $-\int_\Omega N_{5i,y}\mu N_{5j,y}\mathrm{d}\Omega$

4 Numerical results

Finite element interpolations of equal polynomial orders are used for all main variables. The elements employed are general quadrilaterals, with bilinear coordinate mapping and Legendre polynomial based hierarchical shape functions [17]. Denoted by N_{1j}, N_{2j}, N_{3j}, N_{4j} and N_{5j} are the basis functions associated with the double stress components μ_{xxz}, μ_{xyz}, μ_{yxz}, μ_{yyz} and the displacement field w, respectively. The typical block of the total stiffness matrix is shown in Table 1, whereas the typical force vector block is shown in Table 2.

Values of index j ranging from 1 to 4 correspond to the standard bilinear basis functions (i.e., polynomial interpolation order p equals 1). Values of index j greater or equal to 5 are associated with the higher order *hierarchical* basis functions (i.e., $p \geq 2$).

Topologically, the higher order basis functions are of two kinds; *side modes*, which are related to mesh edges and *internal (bubble) modes*, which are related to the interior of the elements. It is noted that the polynomial interpolation order increases without introducing new physical nodes. Moreover, the finite element spaces expand in a hierarchical fashion. When increasing the polynomial order from p to $p + \Delta p$ the previous basis functions (i.e., up to order p) remain and higher order corrections (i.e., of order $p + 1$ up to $p + \Delta p$) are added to the approximation spaces.

In Table 2, $f_z(x, y)$ denotes a body force term [Force/Length^3] which may be added appropriately on the right hand side of the governing Eq. (3.4). Note that, in the current formulation, the number of unknowns could be reduced by imposing the condition $\mu_{xyz} = \mu_{yxz}$, see (2.3). Then the modified stiffness matrix produces the same results as the full stiffness shown in Table 1.

Four different model problems are considered. The first two have linear and bilinear displacement fields and serve as *consistency tests* (or *patch tests*). These examples verify that the proposed mixed finite element formulation captures a linear or bilinear exact solution for arbitrary geometry meshes. The third model problem assumes a fictitious body force $f_z(x, y)$, which results in a smooth exact solution. This example is used to validate the accuracy and convergence of the present implementation scheme in the framework of the p-extension.

Table 2 The force vector of the mixed finite element formulation

$r_{xxz}\,(N_{1i})$	$\int_S N_{1i}\frac{\partial w}{\partial x}n_x\mathrm{d}S$
$r_{xyz}\,(N_{2i})$	0
$r_{yxz}\,(N_{3i})$	0
$r_{yyz}\,(N_{4i})$	$\int_S N_{4i}\frac{\partial w}{\partial y}n_y\mathrm{d}S$
$s\,(N_{5i})$	$-\int_S N_{5i}t_z\mathrm{d}S - \int_\Omega N_{5i}f_z\mathrm{d}\Omega$

Finally, the last example (which is the most interesting) refers to the mode III crack problem in the framework of dipolar strain gradient elasticity. The exact solution for the true stress field is highly singular near the crack tip, varying as $O\left(r^{-3/2}\right)$, within a neighborhood of $O\left(\sqrt{c}\right)$. This model problem verifies the ability of the current mixed formulation to capture the exact solution behaviour at different length scales, provided that proper mesh refinement has been performed.

It is emphasized, that for all model problems, the constants have the proper dimensions, so that the final formulas are dimensionally correct. For example, in model problem 2, $w = 1 \cdot xy$ where 1 must have units [Length^{-1}] or in model problem 3, $w = \sin(2 \cdot \pi x)$, where 2 must also have units [Length^{-1}].

Model problem 1. Linear displacement field (pure Cauchy shear stress state)

The problem geometry and boundary conditions are shown in Fig. 2. The exact solution fields are as follows,

$$u_z = w = My, \quad \mu_{xxz} = \mu_{xyz} = \mu_{yxz} = \mu_{yyz} = 0 \tag{4.1}$$

where $M = \frac{P}{\mu}$ (non-dimensional constant), μ is the standard shear modulus and $t_z = P$ is the applied constant, external, true traction, with units of [Force/Length^2], see (2.2).

For any domain, with dimensions W, H and general quadrilateral meshes of arbitrary polynomial order, the finite element solution coincides with the exact solution. A typical mesh configuration employed in the numerical tests is depicted in Fig. 2.

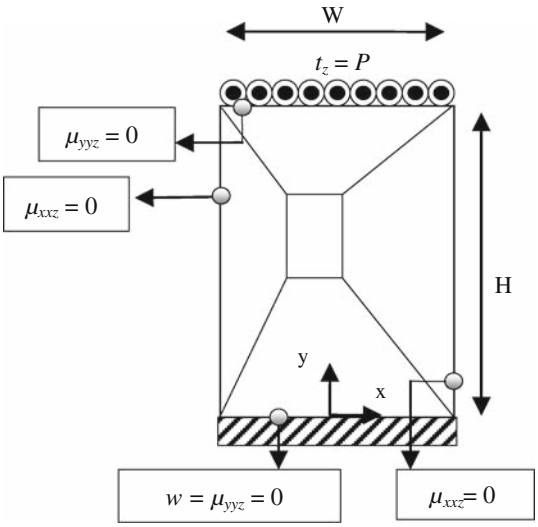

Fig. 2 Typical mesh used for model problem 1 (pure shear stress state)

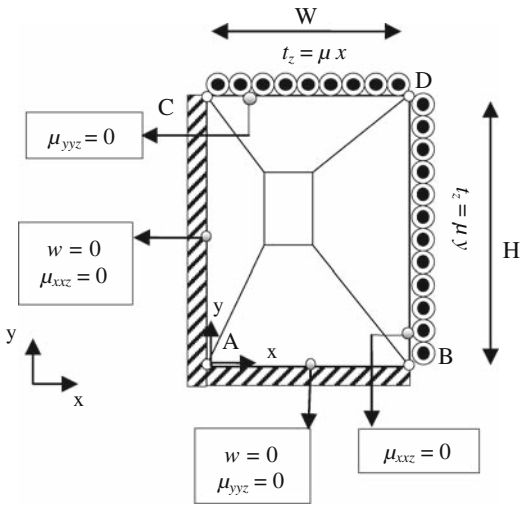

Fig. 3 Typical mesh used for model problem 2 (bilinear displacement field)

Model problem 2. Bilinear displacement field

The problem geometry and boundary conditions are shown in Fig. 3. The exact solution fields are as follows,

$$w = xy \tag{4.2a}$$

$$\mu_{xxz} = 0, \quad \mu_{xyz} = \mu_{yxz} = \mu c, \quad \mu_{yyz} = 0 \tag{4.2b}$$

where c is the gradient coefficient, see (2.3).

The external true tractions along the edges BD and CD are $t_z = \mu y$ and $t_z = \mu x$, respectively, see (2.6) and (2.7). It is also important to note that, due to (4.2b), the jump condition (2.5c), for the right angle at point D, becomes,

$$\mu_{xyz} + \mu_{yxz} = 2\mu c \tag{4.3}$$

Hence, a point load $-2\mu c$ must be added at the fifth block of the force vector for the node located at D, see Appendix I and [13] for more general cases.

For any domain, with dimensions W, H and general quadrilateral meshes of arbitrary polynomial order, the finite element solution essentially coincides with the exact solution. A typical mesh configuration employed in the numerical tests is depicted in Fig. 3.

Model problem 3. Smooth exact solution, based on a fictitious body force.

The boundary value problem and the discretization of the problem domain are shown in Fig. 4. A mesh of 12 general quadrilateral elements is used. The exact solution fields are as follows,

$$w = \sin(2\pi x)y \tag{4.4a}$$

$$\mu_{xxz} = -(2\pi)^2 \mu c y \sin(2\pi x) \tag{4.4b}$$

$$\mu_{xyz} = \mu_{yxz} = (2\pi\mu c)\cos(2\pi x) \tag{4.4c}$$

$$\mu_{yyz} = 0 \tag{4.4d}$$

The body force applied is

$$f_z(x, y) = (2\pi)^2 \mu y \sin(2\pi x) + (2\pi)^4 \mu c y \sin(2\pi x) \tag{4.5}$$

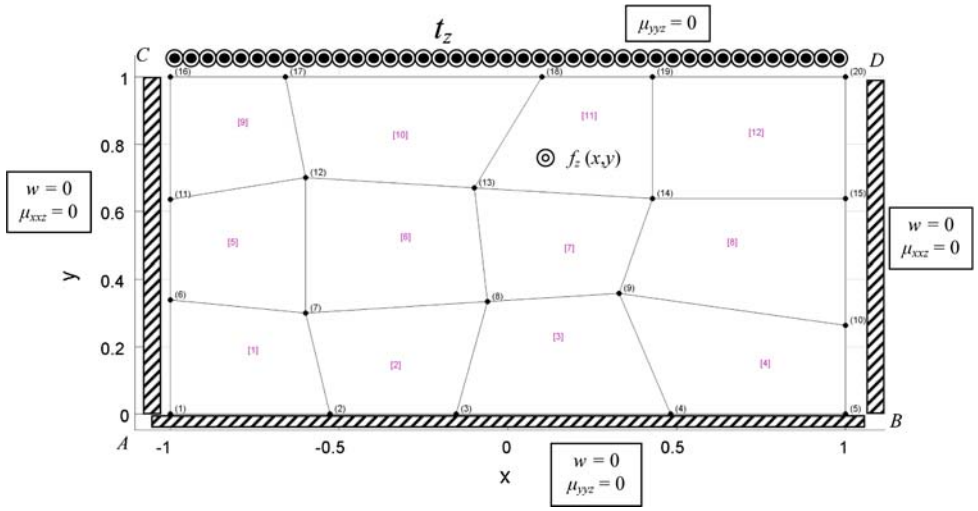

Fig. 4 Mesh used for model problem 3

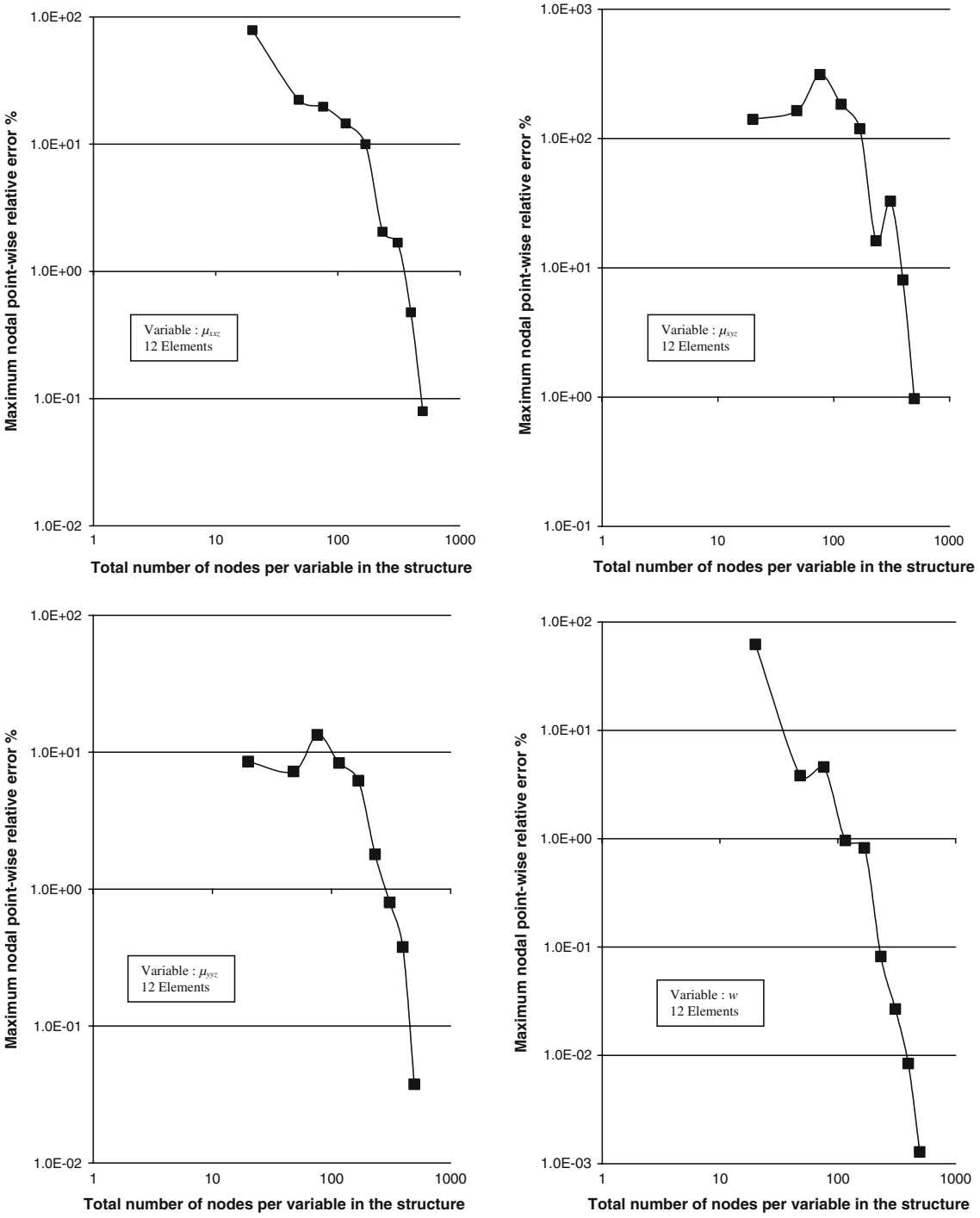

Fig. 5 Maximum nodal relative error convergence, for the main variables. Model problem 3

The true traction applied along edge CD is

$$t_z = \mu \sin(2\pi x) + 2(2\pi)^2 \mu c \sin(2\pi x) \tag{4.6}$$

The problem parameters are,

$$\mu = 100.0 \left[\frac{\text{Force}}{\text{Length}^2}\right], \quad c = 0.00405 \left[\text{Length}^2\right]. \tag{4.7}$$

The convergence of the maximum point-wise relative errors of the main variables at the vertex nodes of the mesh, versus the total number of nodes per variable (including the hierarchical nodes), are depicted in Fig. 5. The relative errors have been evaluated with respect to the maximum exact value of each variable. The only exception is the μ_{yyz} variable for which the maximum exact value of μ_{xxz} has been used.

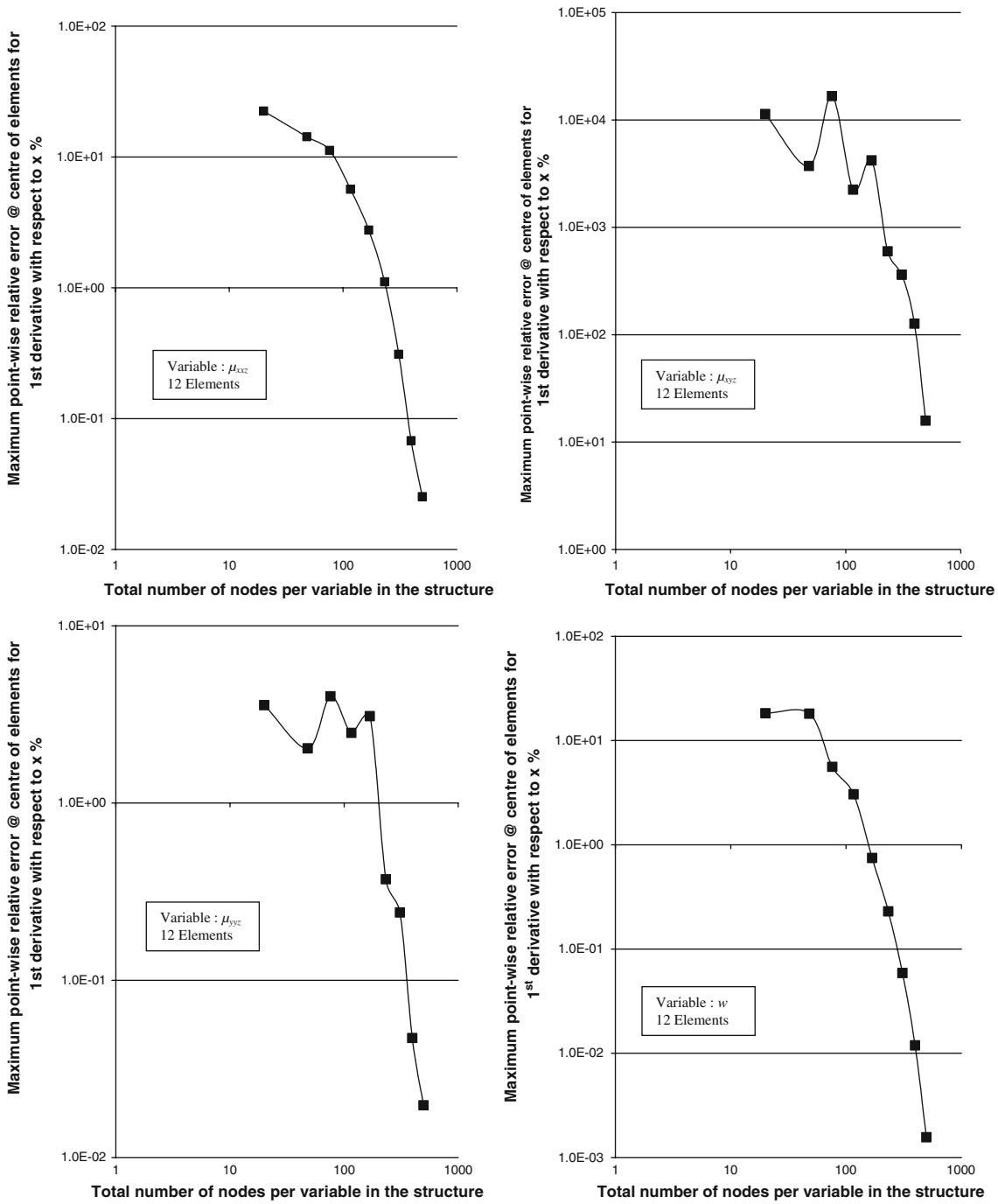

Fig. 6 Maximum point-wise relative error at the centre of the elements for the 1st derivative, of the main variables, with respect to x. Model problem 3

The convergence of the maximum point-wise relative errors of the 1st derivatives with respect to x, at the middle of the elements, are depicted in Fig. 6. Finally, the convergence of the relative errors of the 1st derivatives with respect to y, are depicted in Fig. 7. The relative errors are computed with respect to the maximum point-wise values of the derivatives of the variables. In all of the aforementioned figures logarithmic scale is used for both axes.

In general, it can be said that all variables converge exponentially (typical behaviour in p-extension analyses) when they get past the pre-asymptotic area. The rate of convergence is not the same for all the variables. In particular, the

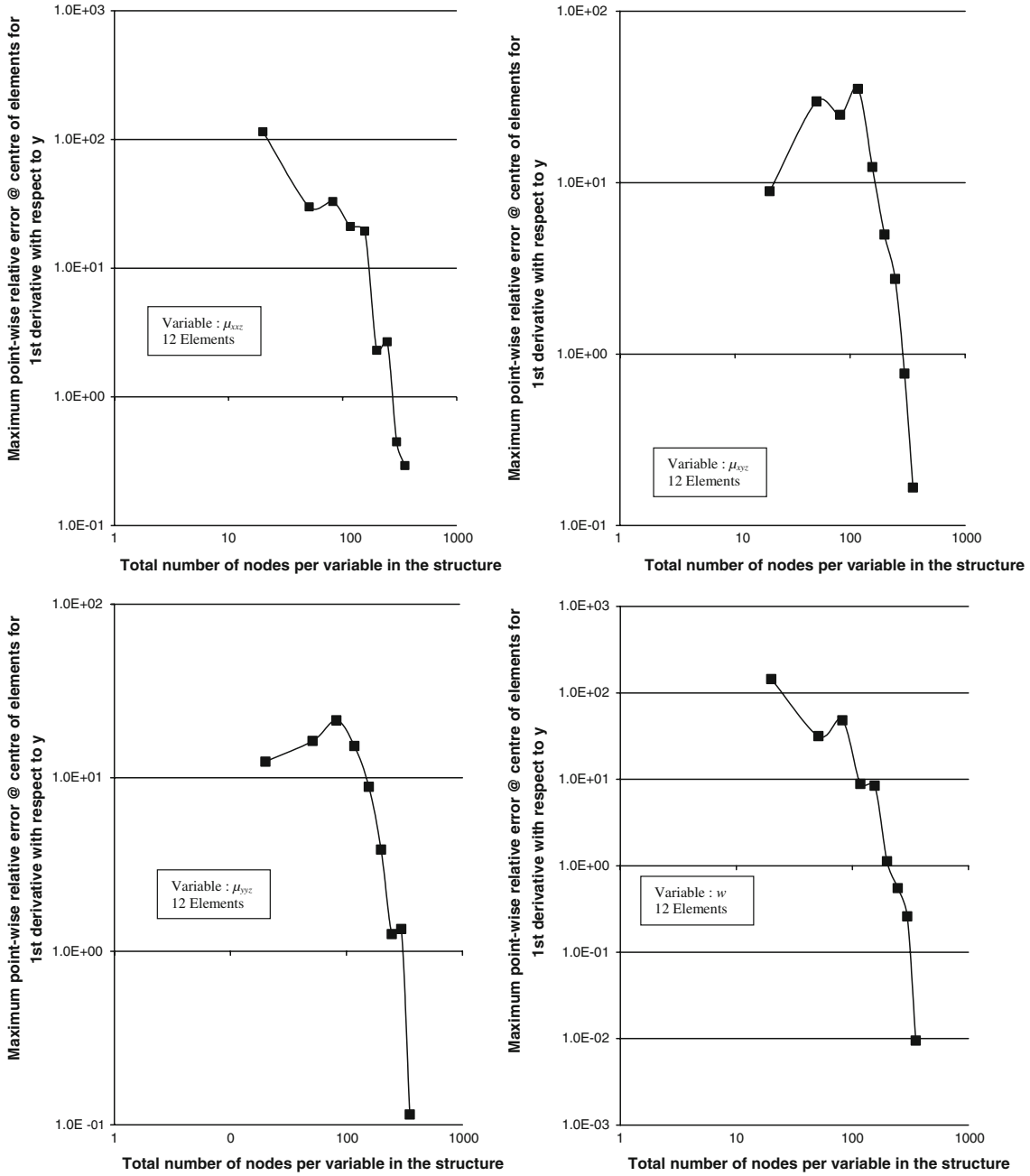

Fig. 7 Maximum point-wise relative error at the centre of the elements for the 1st derivative, of the main variables, with respect to y. Model problem 3

best convergence appears, as expected, for the out-of-plane displacement variable, w.

Model problem 4. Mode III Crack problem in dipolar strain gradient elasticity

The problem geometry and boundary conditions are shown in Fig. 8, see also [7]. Due to the anti-symmetric nature of the problem, the upper right quarter of the total problem domain is analyzed. The dimensions of this quarter are shown in Fig. 9. The problem parameters are $c = 0.005$ [Length^2], $\mu = 100$ [Force/Length^2] and $t_z = P = 10$ [Force/Length^2]. The total length of the crack (20 Length Units) is 1/4 of the total slab width (80 Length Units).

According to theoretical analysis, see [7,19], next to the crack tip, within a neighborhood of radius $O(\sqrt{c})$, the displacement field has an asymptotic behaviour $O(r^{3/2})$, where r is the distance from the crack tip. Away from this neighborhood, but still far from the external boundaries, the exact solution displacements approach the behaviour of the standard Elasticity asymptotic solution, i.e. $O(r^{1/2})$.

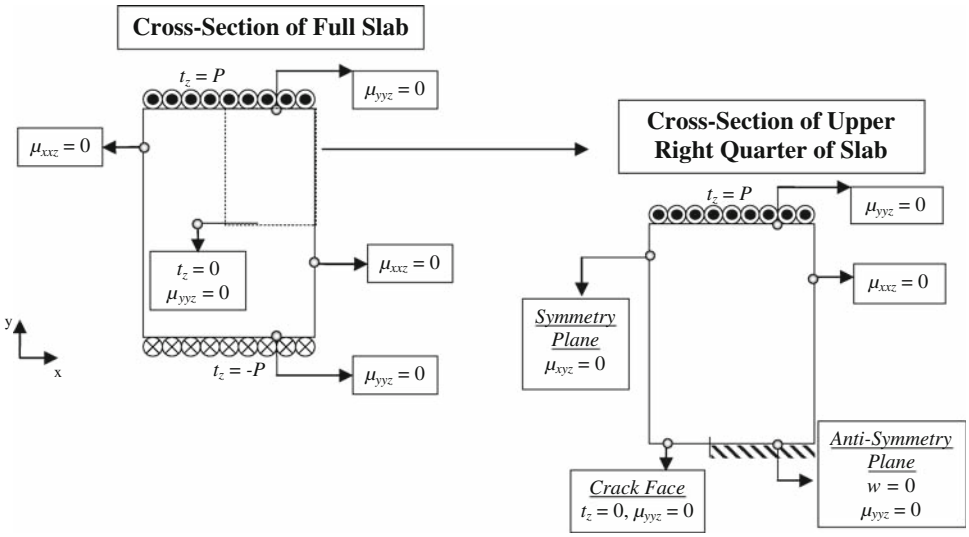

Fig. 8 Boundary value problem of mode III central crack

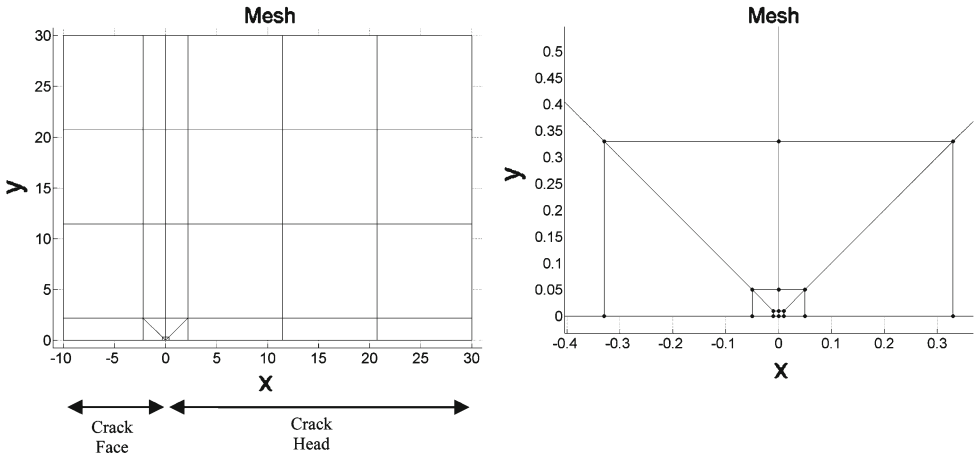

Fig. 9 Mesh used in mode III crack problem (upper right quarter)

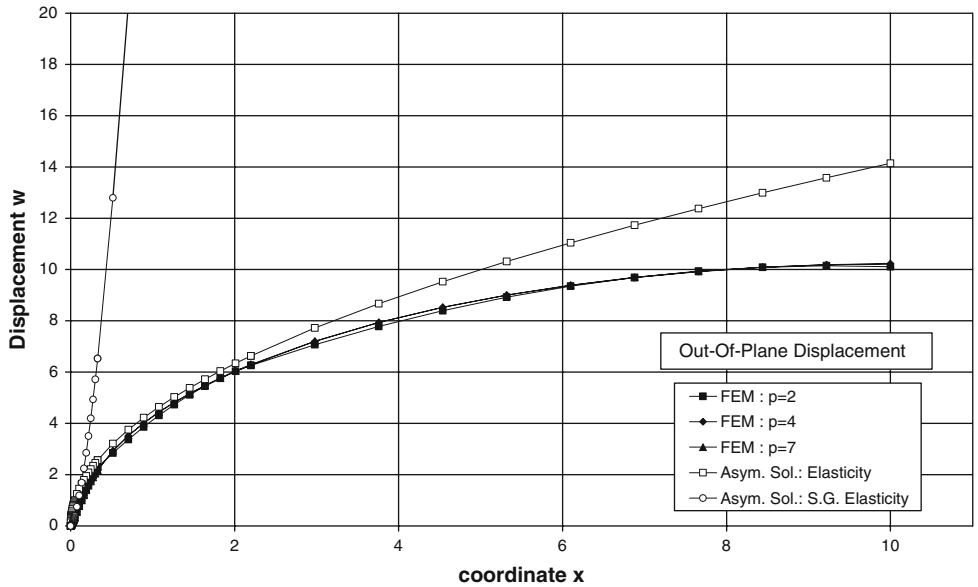

Fig. 10 Displacement field w of the crack face

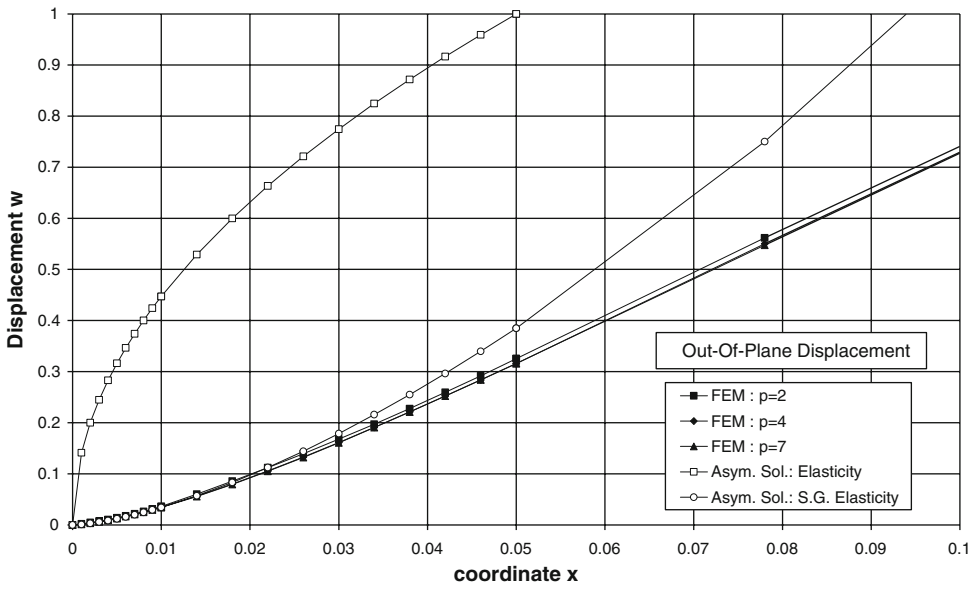

Fig. 11 Detail of Displacement field w, over the crack face, near the crack tip (zoom of Fig. 10)

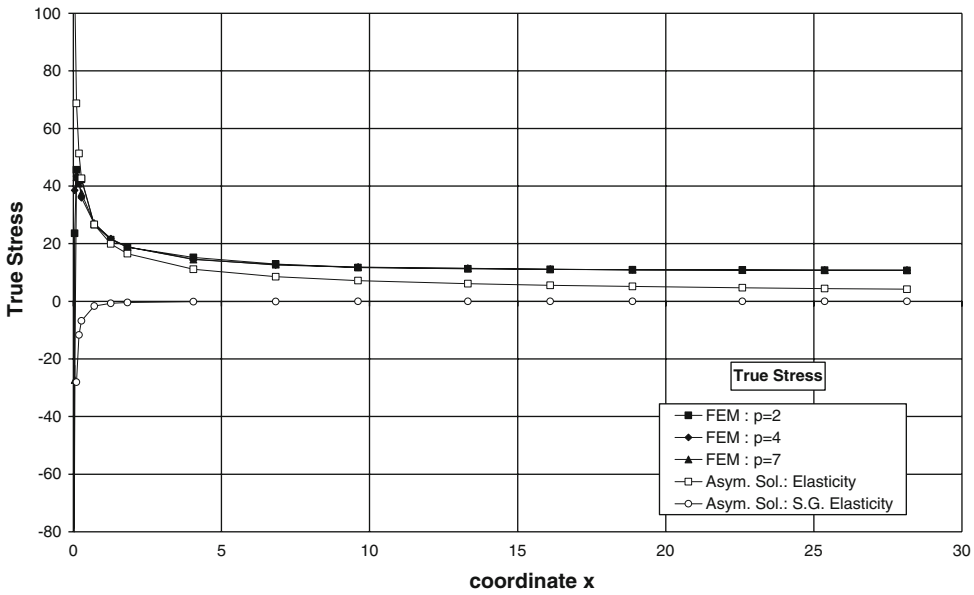

Fig. 12 True stress field in front of the crack tip. Elasticity and gradient solutions compared against Mixed FEM solutions for various p

Moreover, due to gradient effects, the true stress, namely the y component of the true traction on a section parallel to x axis, see (3.6), near the crack tip, has opposite sign from that of the elasticity solution and approaches infinity as $O(r^{-3/2})$. Far from the neighborhood of radius $O(\sqrt{c})$, but still near the crack tip, compared to the problem domain size, the exact solution for the true stress approaches the asymptotic behaviour of the standard elasticity solution, i.e. $O(r^{-1/2})$. Of course, far away from the crack tip, the true stress approaches the stress field applied macroscopically.

All the above are verified by the extensive numerical experimentation carried out in the present work. The mesh employed in the analysis is shown in Fig. 9. Figure 10 shows the displacement field of the crack face, at the macroscopic level, which approaches the shape of the standard elasticity solution. Figure 11 zooms near the crack tip, within the neighborhood of $O(\sqrt{c})$. As predicted by the theoretical asymptotic and full field solution analyses, [7,19], in the vicinity of the crack tip, the crack face displacement demonstrates a cleaving (cusp-like) behaviour, contrary to the classical elasticity displacement field, which is more blunted, see Fig. 11.

For the current mode III crack model problem, the asymptotic displacement and true stress fields for standard and gradient elasticity are given in Appendix II.

Figure 12 depicts the variation of the true stress, ahead of the crack tip, compared to standard elasticity and gradient elasticity asymptotic solutions. As predicted by the full field analysis [7,19] the true stress exhibits a local maximum. Then it reduces, changes sign and becomes infinite within a neighborhood of $O(\sqrt{c})$, see Fig. 13.

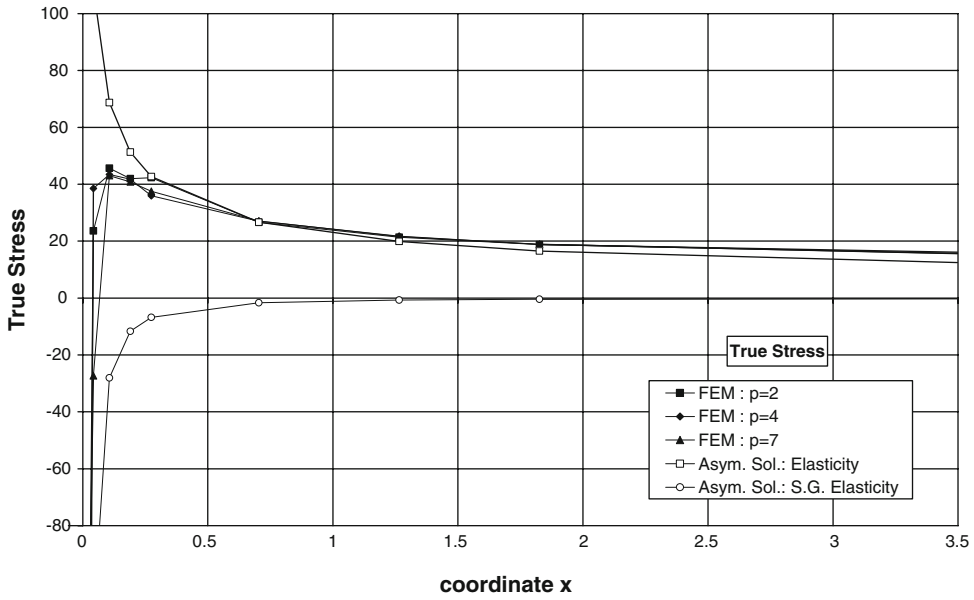

Fig. 13 True stress field in front of the crack tip (zoom of Fig. 12)

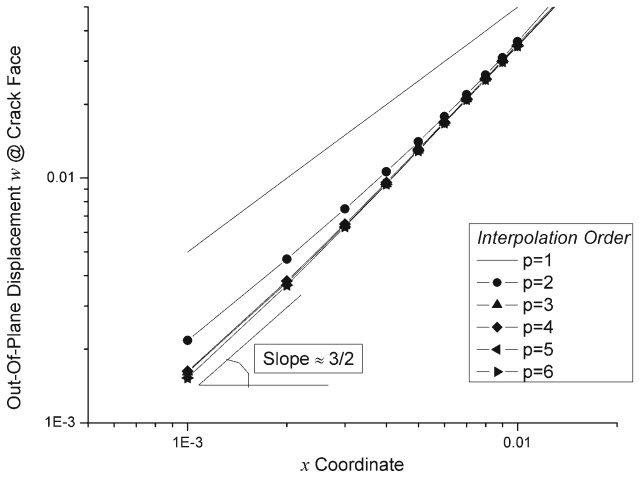

Fig. 14 FEM solution of the out-of-plane displacement field w of the crack face near the crack tip, for various interpolation orders (Log–Log axes)

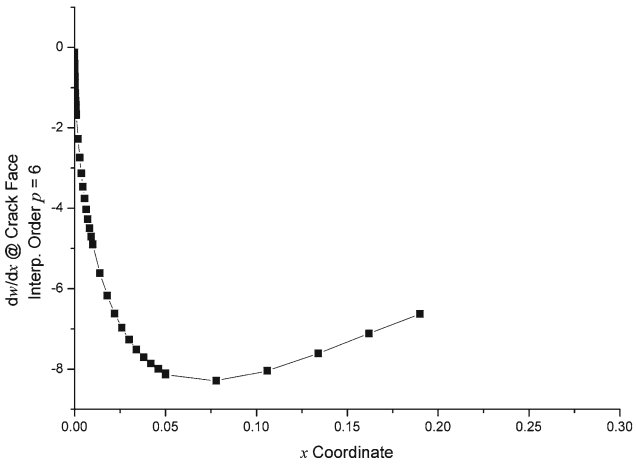

Fig. 15 FEM solution of the 1st derivative of out-of-plane displacement field with respect to x at the crack face near the crack tip, for interpolation order $p = 6$

The Log–Log Fig. 14 depicts the FEM displacement distribution at the crack face, near the crack tip. Figures 15 and 16 show the distribution of the partial derivative of the displacement with respect to x(strain γ_{xz}), at the crack face near the crack tip and its Log–Log plot, respectively. Last but not least, Fig. 17 shows the Log–Log plot of the *true stress* at the crack head, near the crack tip. All of these Log–Log plots verify the respective asymptotical r dependence of each variable, which have been stated above.

5 Conclusions

A mixed formulation has been developed and numerically tested for the general 2D anti-plane shear problem, in the framework of *dipolar strain gradient elasticity* (form II). The current formulation employs the double stress components and the displacement field as main variables ($\mu - u$ formulation, [12]). High order, C^0-continuous, conforming basis functions were used in the finite element approximation (p-extension), with equal polynomial interpolation order for all main variables.

The numerical examples demonstrate the accuracy and effectiveness of the proposed mixed method, in terms of error convergence versus the number of degrees of freedom. The results for the mode III crack problem reveal that, with proper mesh refinement near the crack tip, the current method is capable of capturing the exact solution features at several length scales. Theoretical predictions for the mode III crack problem are verified [7,19], namely, that the true stress near

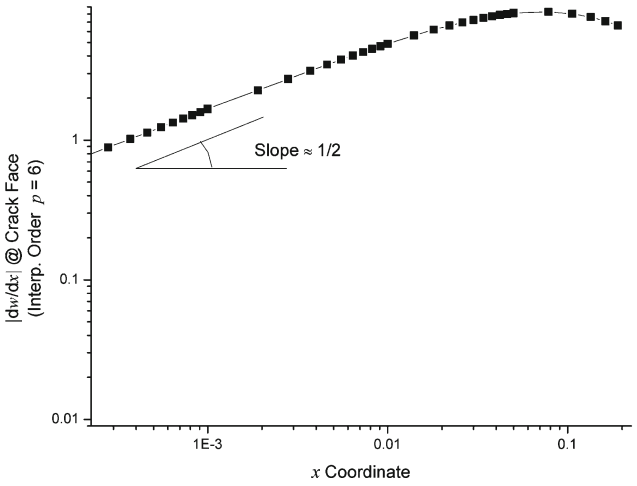

Fig. 16 FEM solution of the 1st derivative of out-of-plane displacement field with respect to x for interpolation order $p = 6$ (Log–Log axes)

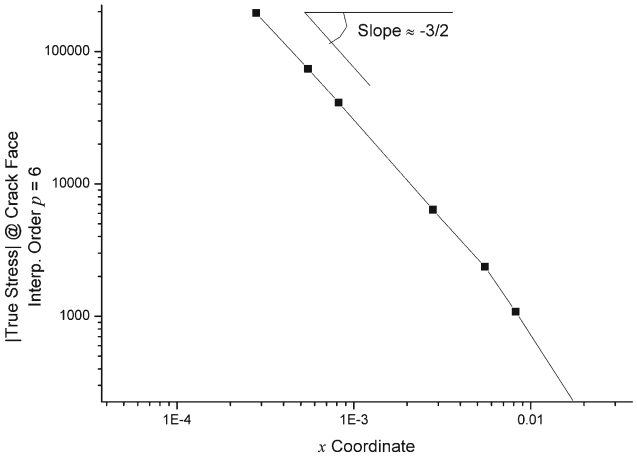

Fig. 17 FEM solution of the true stress field at the crack head near the crack tip for interpolation order $p = 6$ (Log–Log axes)

the crack tip exhibits a local maximum within a neighborhood of the order of the characteristic size of the material microstructure.

For practical purposes, this local maximum value may serve as a measure of the critical stress level at which further advancement of the crack may occur. Also, it may be used to develop certain failure criteria for the given structure, see [7] for a more comprehensive discussion. Finally, as predicted by the theoretical asymptotic (and full field solution) analyses, in the vicinity of the crack tip, the crack face displacement exhibits a cusp-like behaviour, as compared to classical elasticity predictions of a more blunted front.

Future research directions could be the development and numerical investigation of similar mixed formulations for plane stress and strain problems in the framework of gradient elasticity as well as full 3D numerical models. Finally, since the effectiveness of the approximate solutions is improved dramatically with proper mesh refinements, the development of *a posteriori error estimators* and *adaptive techniques* is necessary to reduce the error at high-gradient regions, with as low computational cost, as possible.

Acknowledgments This work was conducted within the framework of the EPEAEK program "Pythagoras II". The Project is co-funded by the European Social Fund (75%) and National Resources (25%).

Appendix I: Deduction of the jump condition at right angle corners, for the anti-plane shear problem

The starting point is a more general version of (2.5c), see [4,13,14],

$$[m_j n_i \mu_{ijk}] = [m_j T_{jk}] \quad \text{on } C \tag{I.1}$$

where T_{jk} denotes the externally applied double traction components (if any).

The above relation holds for cases of non-zero jump condition (e.g., model problem 2, Sect. 4). Then, in our mixed formulation, point load terms must be added to the force vector, corresponding to the nodes at the corners, see (3.8), (3.9) and (3.11). The formal analysis of the general 3D formulation is given in [13]. In 3D scenarios, when $[m_j T_{jk}] \neq 0$, distributed line loads (along curve C) are added in the force vector.

Consider now a right angle corner of the boundary. Recall that $m_j := e_{lkj} s_l n_k$, where s_l denotes the components of the tangential vector of curve C. The problem domain is two-dimensional, nevertheless, the respective 3D body has the form of a thick slab along z-direction. Hence, the respective curve C is actually a line, parallel to z-axis, which passes from the given corner point (e.g., $s_1 = s_2 = 0$ and $s_3 = 1$)

We are now in the position to write extensively $m_j = e_{lkj} s_l n_k$. Without affecting the generality, we consider an upper right corner (e.g., point D in Fig. 3). Then, for the side which is parallel to the y-axis we have $n_1 = 1$ and $n_2 = n_3 = 0$ and

$$m_j = e_{3kj} s_3 n_k = e_{31j} s_3 n_1 = e_{31j} \tag{I.2}$$

Based on the definition of the alternating tensor e_{lkj}, $m_1 = m_3 = 0$ and $m_2 = 1$. Therefore, for the side which is parallel to the y-axis,

$$m_j n_i \mu_{ijk} = m_2 n_i \mu_{i2k} = m_2 n_1 \mu_{12k} = \mu_{12k} \tag{I.3}$$

Based on the hypotheses of the anti-plane shear model, (I.3) is meaningful only for $k = 3$. Resuming, for the side which is parallel to the y-axis, the terms in the brackets of (I.1) reduce to

$$m_j n_i \mu_{ijk} = \mu_{123} = \mu_{xyz} \tag{I.4a}$$

$$m_j T_{jk} = T_{23} = T_{yz} \tag{I.4b}$$

Next, we focus attention on the side which is parallel to the x-axis ($n_1 = n_3 = 0$ and $n_2 = 1$),

$$m_j = e_{3kj} s_3 n_k = e_{32j} s_3 n_2 = e_{32j} \tag{I.5}$$

From (I.5), there follows $m_2 = m_3 = 0$ and $m_1 = -1$. Therefore, for the side which is parallel to the x-axis,

$$m_j n_i \mu_{ijk} = m_1 n_i \mu_{i1k} = m_1 n_2 \mu_{21k} = -\mu_{21k} \tag{I.6}$$

Once again, (I.6) is meaningful only for $k = 3$. Resuming, for the side which is parallel to the x-axis, the terms in the brackets of (I.1) reduce to

$$m_j n_i \mu_{ijk} = -\mu_{213} = -\mu_{yxz} \tag{I.7a}$$

$$m_j T_{jk} = -T_{13} = -T_{xz} \tag{I.7b}$$

Based on the definition of the bracket operator $[*]$, see Sect. 2 and [3,14], from (I.4) and (I.7), the following jump condition at the right angle corners is deduced,

$$\mu_{xyz} + \mu_{yxz} = T_{yz} + T_{xz} \tag{I.8}$$

In the practical case where $T_{yz} = T_{xz} = 0$, (I.8) leads to (2.13). The latter has been employed in the formation of (3.8). Finally, recall that $\mu_{xyz} = \mu_{yxz}$, due to double stress definitions, see (2.3b, c). Therefore, $T_{yz} = T_{xz} = 0$ gives $\mu_{xyz} = \mu_{yxz} = 0$ at the right angle corners.

Appendix II : Mode III crack problem—asymptotic fields near the crack tip

Asymptotic displacement fields at the crack face:

Standard elasticity

$$w(r) = \frac{K_{\mathrm{III}}}{\mu}\sqrt{\frac{2r}{\pi}}\,[\mathrm{Length}] \tag{II.1}$$

where for the given model problem of Sect. 4, $\mu = 100$ [Force/Length^2] and

$$K_{\mathrm{III}} \approx P\sqrt{\pi\alpha}, \quad \alpha \text{ is half-crack length.} \tag{II.2}$$

Hence for the given problem

$$K_{\mathrm{III}} \approx 10\sqrt{10\pi} = 56.0499\,[\mathrm{Force}\cdot\mathrm{Length}^{-3/2}] \tag{II.3}$$

Gradient elasticity [7]

$$w(r) = Br^{3/2}\,[\mathrm{Length}] \tag{II.4}$$

where

$$B = \frac{8K_{\mathrm{III}}}{3\mu\sqrt{2c}\sqrt{6\pi}} = 3.44265\,[\mathrm{Length}^{-1/2}] \tag{II.5}$$

Asymptotic true stress fields at the crack head, near the crack tip

Standard elasticity

$$t_{yz} = \frac{K_{\mathrm{III}}}{\sqrt{2\pi r}} = 22.3606 r^{-1/2}\,[\mathrm{Force}\cdot\mathrm{Length}^{-2}] \tag{II.6}$$

Gradient elasticity [7]

$$t_{yz} = \frac{\sqrt{3c}K_{\mathrm{III}}}{4\sqrt{\pi}} r^{-3/2} = 0.96824 r^{-3/2}\,[\mathrm{Force}\cdot\mathrm{Length}^{-2}] \tag{II.7}$$

References

1. Amanatidou E, Aravas N (2002) Mixed finite element formulations of strain-gradient elasticity problems. Comput Methods Appl Mech Eng 191:1723–1751
2. Bathe KJ (2001) The inf–sup condition and its evaluation for mixed finite element method. Comput Struct 79:243–252
3. Bhattacharyya PK, Nataraj N (2002) Error estimates for isoparametric mixed finite element solution of 4th order elliptic problems with variable coefficients. Comput Mech 28:435–455
4. Bleustein JL (1967) A note on the boundary conditions of Toupin's strain-gradient theory. Int J Solids Struct 3:1053–1057
5. Braess D (1997) Finite elements. Cambridge University Press, UK
6. Brezzi F, Bathe KJ (1990) A discourse on the stability conditions for mixed finite element formulations. Comput Methods Appl Mech Eng 82:27–57
7. Georgiadis HG (2003) The mode III crack problem in microstructured solids governed by dipolar gradient elasticity: Static and dynamic anlaysis. J Appl Mech 70:517–530
8. Giannakopoulos AE, Stamoulis K (2007) Structural analysis of gradient elastic components. Int J Solids Struct 44:3440–3451
9. Gourgiotis PA, Georgiadis HG (2007) Distributed dislocation approach for cracks in couple-stress elasticity: shear modes. Int J Fract 147:83–102
10. Karlis GF, Tsinopoulos SV, Polyzos D, Beskos DE (2007) Boundary element analysis of mode I and mixed mode (I and II) crack problems of 2-D gradient elasticity. Comput Methods Appl Mech Eng 196:5092–5103
11. Lam DCC, Yanga F, Chonga ACM, Wanga J, Tong P (2003) Experiments and theory in strain gradient elasticity. J Mech Phys Solids 51:1477–1508
12. Markolefas S, Tsouvalas DA, Tsamasphyros GI (2008) Some C°-continuous mixed formulations for general dipolar linear gradient elasticity boundary value problems and the associated energy theorems. Int J Solids Struct 45:3255–3281
13. Markolefas SI, Tsouvalas DA, Tsamasphyros GI (2007) Theoretical analysis of a class of mixed, C^0 continuity formulations for general dipolar gradient elasticity boundary value problems. Int J Solids Struct 44:546–572
14. Mindlin RD (1964) Micro-structure in linear elasticity. Arch Rat Mech Anal 16:51–78
15. Mindlin RD, Eshel NN (1968) On first-gradient theories in linear elasticity. Int J Solids Struct 4:109–124
16. Polyzos D, Tsepoura KG, Tsinopoulos SV, Beskos DE (2003) A boundary element method for solving 2-D and 3-D static gradient elastic problems. Part I. Integral formulation. Comput Methods Appl Mech Eng 192:2845–2873

17. Szabo B, Babuška I (1991) Finite element analysis. Wiley, New York
18. Tsamasphyros GI, Markolefas S, Tsouvalas DA (2007) Convergence and performance of the h- and p-extensions with mixed finite element C^0-continuity formulations, for tension and buckling of a gradient elastic beam. Int J Solids Struct 44:5056–5074
19. Zhang L, Huang Y, Chen JY, Hwang KC (1998) The mode III full-field solution in elastic materials with strain gradient effects. Int J Fract 92:325–348